A Numerical Study on Path of the Kuroshio with Reference to Genera-tion of Smoll Meanders Southeast of Kyushu

Sci. Rep. Tôhoku Univ., Ser. 5, (Tôhoku Geophys. Journ.), Vol. 27, No. 2, pp. 39–55, 1980.

A Numerical Study on Path of the Kuroshio with Reference to Generation of Small Meanders Southeast of Kyushu

YOSHIHIKO SEKINE and YOSHIAKI TOBA

Geophysical Institute, Faculty of Science
Tôhoku University, Sendai 980, Japan

(Received July, 18, 1980)

Abstract: Path dynamics of the Kuroshio between Satsunan region and Kii Channel is investigated numerically, for the study of the generation of small meanders southeast of Kyushu. A two layer model with inflow and outflow system is assumed. The topographies corresponding to the south and eastern coast of Kyushu, the southern coast of Shikoku, and their offshore regions are simplified in the modelling so that only the main topographic features are represented. A quasi-stationary flow pattern of the Kuroshio exists in a state where the lower layer velocity is still a few percent of the upper layer one, and there is little possibility of occurrence of the small meander. Dynamical factors confining the Kuroshio path along the continental margin are the bottom topographic effect of the continental slope and the westward intensification due to the latitudinal variation of Coriolis parameter, and under the above conditions the former contribution is much more important than the latter. As the dynamical cause to overcome both the effects for the generation of the small meander, unstationary process including the variation of mass transport is proposed.

1. Introduction

Over the last thirty years, observations have disclosed the existence of two typical paths of the Kuroshio south of Japan (Stommel and Yoshida, 1971). One of the paths includes a quasi-stationary large meander accompanied by a large cold water mass to the south of Honshu. Since the Izu ridge presents a conspicuous bottom characteristic particular to this region of the western boundary of the Pacific Ocean, some studies by numerical models including this ridge have been attempted (e.g., Endoh, 1973, 1978; Sekine, 1979), assuming that the bottom effect of the Izu ridge may play an essential role on the path dynamics of the Kuroshio. White and McCreary (1976) also considered the ridge for a gate effect in their path-dynamical model. To this date, main emphasis of the dynamical investigation with respect to the Kuroshio path has been given on the understanding of the stationary meander and the bimodal character. However, theoretical aspects of the process of formation and disappearance of the stationary meander have not yet been clarified well.

On the other hand, it is also well known that prior to the formation of a stationary meander, a small meander is generated southeast of Kyushu, and it moves eastward to develop to the stationary meander. Fig. 1 displays the changes in the Kuroshio path showing this process according to Shoji (1972). Stationary large meanders formed in

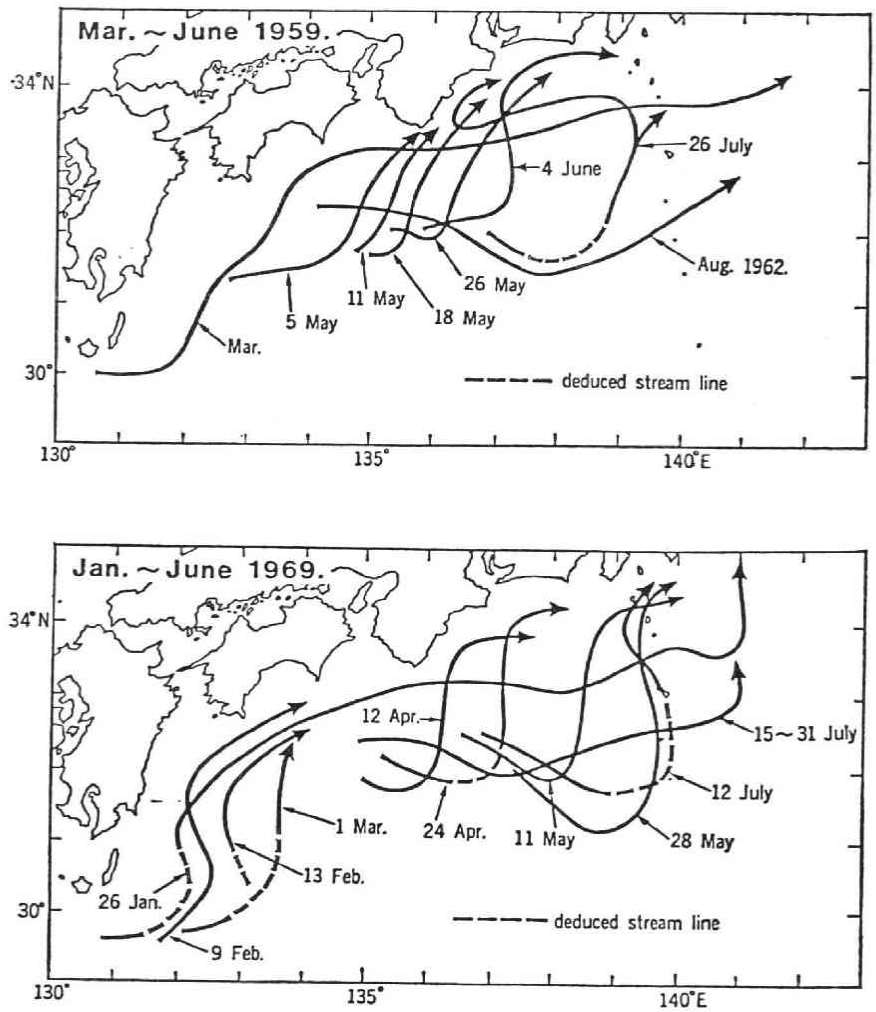

Fig. 1. Generation and evolution of the small meanders of the Kuroshio: Some examples (after Shoji, 1972).

1953, 1959, 1969, and 1975 were all preceded by this sort of small meanders. This small meanders may thus be considered as a transient phenomenon before the formation of the stationary meanders.

The observational properties of these small meanders were summarized in Shoji (1972), Nitani (1975), and Solomon (1978). Moriyasu (1961) examined the relations between the wind stress due to the winter monsoon off southern Kyushu and the shift of current axis offshore by the coastal upwelling. Fukuoka (1960) studied the deflection of current direction due to the oceanic ridge at Tokara straight by use of the lee wave theory proposed by Bolin (1950).

As a first step of approach from the point of view that the large stationary meander of the Kuroshio evolves from this small meander, dynamical conditions behind the occurrence of the small meanders are investigated in the present article numerically,

with a close look at the path dynamics of the Kuroshio in this region. Since the space scale of the small meanders during their generation is smaller than one-third of the stationary meander, and since the emphasis of this study is laid upon the occurrence of these small meanders, the local dynamics associated with the bottom and coastal topographies only of Kyushu and Shikoku are considered here.

As a result, it will be shown that the separation of the current path from the continental margin in the form of the small meanders can not take place in the quasi-stationary state, and it will be inferred that this meander can be generated only in an unstationary process such as variation of the mass transport. An extension of the present work including the Izu ridge are left for a future study.

2. Dynamical Model

The dynamical model employed in the present study is shown schematically in Fig. 2. These topographies are reasonably simplified so that the main features are well represented. The basin is rectangular and has a continental slope of a constant gradient. The northern and western boundaries correspond to the coastal lines of Shikoku and Kyushu, respectively. The southern and eastern boundaries are artificial, on which the inward and outward flows are given as the boundary condition.

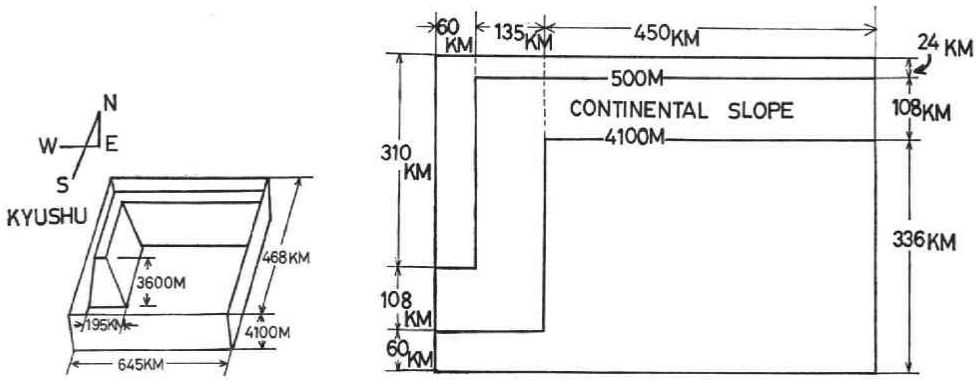

Fig. 2. Schematic view of the model ocean (a) and isopleths of the depth (b).

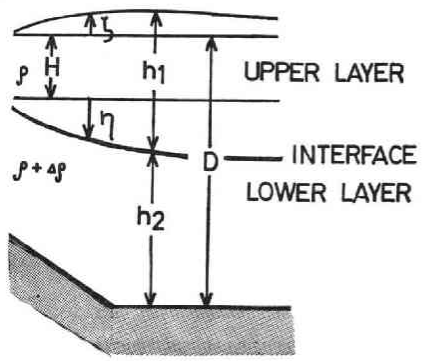

Fig. 3. Schematic diagram of the two layer model showing the density and thickness of each layer.

A two layer model is assumed and the density of the upper and lower layers is ρ and $\rho+\Delta\rho$ and the thickness of the two layers is h_1 and h_2, respectively (see Fig. 3). Let x, y and z be the eastward, the northward and the vertical coordinates, respectively.

Assuming the hydrostatic balance in the vertical direction and the Boussinesq approximation, the horizontal equations of motion and of continuity for the upper and lower layers are given as follows:

$$\frac{\partial u_1}{\partial t} = -\frac{\partial u_1^2}{\partial x} - \frac{\partial u_1 v_1}{\partial y} - \frac{\rho}{\rho_0} g \frac{\partial \zeta}{\partial x} + f v_1 + A_h \nabla^2 u_1 , \tag{1}$$

$$\frac{\partial v_1}{\partial t} = -\frac{\partial u_1 v_1}{\partial x} - \frac{\partial v_1^2}{\partial y} - \frac{\rho}{\rho_0} g \frac{\partial \zeta}{\partial y} - f u_1 + A_h \nabla^2 v_1 , \tag{2}$$

$$\frac{\partial h_1}{\partial t} = -\frac{\partial h_1 u_1}{\partial x} - \frac{\partial h_1 v_1}{\partial y} , \tag{3}$$

and

$$\frac{\partial u_2}{\partial t} = -\frac{\partial u_2^2}{\partial x} - \frac{\partial u_2 v_2}{\partial y} - \frac{\rho}{\rho_0} g \frac{\partial \zeta}{\partial x} + \frac{\Delta\rho}{\rho_0} g \frac{\partial \eta}{\partial x} + f v_2 + A_h \nabla^2 u_2 , \tag{4}$$

$$\frac{\partial v_2}{\partial t} = -\frac{\partial u_2 v_2}{\partial x} - \frac{\partial v_2^2}{\partial y} - \frac{\rho}{\rho_0} g \frac{\partial \zeta}{\partial y} + \frac{\Delta\rho}{\rho_0} g \frac{\partial \eta}{\partial y} - f u_2 + A_h \nabla^2 v_2 \tag{5}$$

$$\frac{\partial h_2}{\partial t} = -\frac{\partial u_2 h_2}{\partial x} - \frac{\partial v_2 h_2}{\partial y} , \tag{6}$$

respectively. In these equations, the subscripts 1 and 2 refer to the upper and the lower layers, respectively, u and v are the eastward and the northward depth-mean velocity components, ρ_0 is the mean density over the whole depth, ∇^2 the horizontal Laplacian operator, g the acceleration of gravity and A_h the coeffidient of eddy viscosity taken as constant of 2.0×10^7 cm^{2}s^{-1}, ζ and η are the surface and interface deviations from the mean levels defined as

$$h_1 = H+\eta , \quad \zeta \ll \eta , \tag{7}$$

$$h_2 = D-H-\eta , \tag{8}$$

and where H is the mean thickness of the upper layer taken to be 400 m and D the total depth of the model ocean. The bottom and interfacial frictions are neglected. The $\Delta\rho$ the difference of density between the two layers is taken as 2.0×10^{-3} g cm^{-3}, and the Coriolis parameter $f=f_0+\beta y$ has a value given by $f_0=7.3\times10^{-5}$s^{-1} and $\beta=1.95\times10^{-13}$ s^{-1}cm^{-1}.

To solve the simultaneous partial differential equations, we assume the rigid lid approximation for the elimination of the external gravity wave. Then eqs. (1)–(6) are transformed to obtain the vorticity equation for vertically integrated flow, and the shear equation for baroclinic mode. This transformation is the conventional method used in the mathematical treatment of two layer model adopted, e.g., by Suginohara

(1973), Holland and Linn (1976), and Miura and Suginohara (1980). The vorticity equation and the shear equation in term of symbols may be expressed in the following forms:

(1) Vorticity equation:

$$LTC = NOL + BET + TOP + COP + FRI\,, \tag{9}$$

where

$$LTC = \frac{\partial z}{\partial t}\,,$$

$$NOL = -\frac{\partial}{\partial x}\left\{\frac{1}{D}\left(\frac{\partial u_1 v_1 h_1}{\partial x} + \frac{\partial v_1{}^2 h_1}{\partial y}\right)\right\} + \frac{\partial}{\partial y}\left\{\frac{1}{D}\left(\frac{\partial u_1{}^2 h_1}{\partial x} + \frac{\partial u_1 v_1 h_1}{\partial y}\right)\right\}$$
$$- \frac{\partial}{\partial x}\left\{\frac{1}{D}\left(\frac{\partial u_2 v_2 h_2}{\partial x} + \frac{\partial v_2{}^2 h_2}{\partial y}\right)\right\} + \frac{\partial}{\partial y}\left\{\frac{1}{D}\left(\frac{\partial u_2{}^2 h_2}{\partial x} + \frac{\partial u_2 v_2 h_2}{\partial y}\right)\right\},$$

$$BET = -\beta \frac{1}{D}\frac{\partial \phi}{\partial x}\,,$$

$$TOP = -f\left\{-\frac{\partial}{\partial x}\left(\frac{1}{D}\frac{\partial \phi}{\partial y}\right) + \frac{\partial}{\partial y}\left(\frac{1}{D}\frac{\partial \phi}{\partial x}\right)\right\},$$

$$COP = \frac{\Delta\rho}{\rho_0} g\left\{\frac{\partial}{\partial x}\left(\frac{h_2}{D}\frac{\partial \eta}{\partial y}\right) - \frac{\partial}{\partial y}\left(\frac{h_2}{D}\frac{\partial \eta}{\partial x}\right)\right\},$$

$$FRI = A_h \nabla^2 z\,,$$

and where

$$z = \frac{\partial}{\partial x}\left(\frac{1}{D}\frac{\partial \phi}{\partial x}\right) + \frac{\partial}{\partial y}\left(\frac{1}{D}\frac{\partial \phi}{\partial y}\right),$$

and ϕ is the transport function defined by

$$u_1 h_1 + u_2 h_2 = -\frac{\partial \phi}{\partial y}\,,$$

$$v_1 h_1 + v_2 h_2 = \frac{\partial \phi}{\partial x}\,.$$

(2) Shear equation of X component:

$$STX = PGX + FVX + NOX + FRX\,, \tag{10}$$

where

$$STX = \frac{\partial S_u}{\partial t}\,,$$

$$PGX = -\frac{\Delta\rho}{\rho_0} g \frac{\partial \eta}{\partial x}\,,$$

$$FVX = fS_v\,,$$

$$NOX = -\frac{\partial u_1^2}{\partial x} - \frac{\partial u_1 v_1}{\partial y} + \frac{\partial u_2^2}{\partial x} + \frac{\partial u_2 v_2}{\partial y},$$

$$FRX = A_h \nabla^2 S_u,$$

and where

$$S_u = u_1 - u_2, \qquad S_v = v_1 - v_2.$$

(3) Shear equation of Y component:

$$STY = PGY + FUY + NOY + FRY, \tag{11}$$

$$STY = \frac{\partial S_v}{\partial t},$$

$$PGY = -\frac{\Delta\rho}{\rho_0} g \frac{\partial \eta}{\partial y},$$

$$FUY = -f S_u,$$

$$NOY = -\frac{\partial u_1 v_1}{\partial x} - \frac{\partial v_1^2}{\partial y} + \frac{\partial u_2 v_2}{\partial y} + \frac{\partial v_2^2}{\partial y},$$

$$FRY = A_h \nabla^2 S_v.$$

The continuity equation for the above equations is

$$\frac{\partial \eta}{\partial t} = \frac{\partial h_2 u_2}{\partial x} + \frac{\partial h_2 v_2}{\partial y}. \tag{12}$$

Eventually, we consider the eqs. (9)–(12) for unknowns z, ϕ, S_u, S_v and η instead of u_1, v_1, h_1, u_2, v_2 and h_2.

The viscous boundary condition is imposed at lateral boundaries. The interface displacements at the inflow and outflow boundaries are given so as to satisfy the geostrophic isostasy, i.e. the inflow and outflow are confined to the upper layer, as

$$\frac{\partial \eta}{\partial y} = -\frac{f}{g^*} u_1, \tag{13}$$

where $g^* = (\Delta\rho/\rho_0)\, g$ is the reduced gravity, and the lateral distributions of inflow and outflow velocity have a type of

$$u_1 = u_0 \sin \frac{\Pi}{L} y, \tag{14}$$

where u_0 is the maximum velocity at the center of the flow and L is the width of the current.

The initial conditions are indicated in Fig. 4. The simultaneous eqs. (9)–(14) are solved numerically. Numerical schemes used in this study are similar to those by Suginohara (1973). The interval of the neighbouring two grid points is 12 km (south-north) and 15 km (west-east). A leap frog scheme is used in the finite form for the

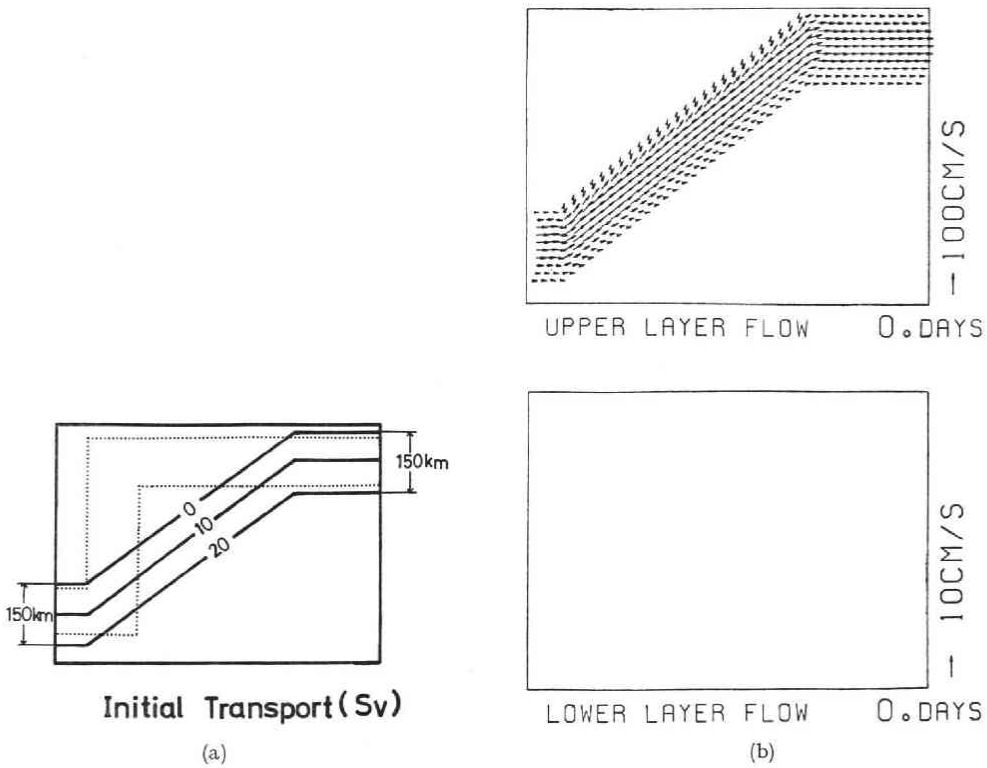

Fig. 4. Initial stream function (a) and initial distribution of velocity for upper and lower layers (b).

Table 1. The parameters and model conditions for experiments to investigate the stationary path of the Kuroshio.

Run No.	Reduced gravity (cm^1s^{-2})	β ($cm^{-1}s^{-1}$)	Continental slope	Remarks
1	1.91	1.95×10^{-13}	existing	Basic Model
2	0	1.95×10^{-13}	non existing	
3	1.91	0.0	existing	
4	0	1.95×10^{-13}	existing	

local time change term with a time step of 2160 s. For the depression of the computational mode in the time development, we used an Euler backward scheme at several intervals among the leap frog scheme (Matsuno, 1966).

In addition to the basic model described above, some other models are employed in order to see specific contributions of various parameters representing respective physical properties. They are shown in Table 1 together with the basic model, Run 1. The influence of the bottom topography is extracted in Run 2, the planetary β effect in Run 3 and the density stratification in Run 4. The initial conditions for these cases are the same as those of Run 1.

3. Results

Fig. 5 shows the sequential patterns of the transport function ϕ for the basic model (Run 1). The interval between the two isopleths is $2.5 \times 10^6 \mathrm{m^2 s^{-1}}$, or 2.5 Sv. The

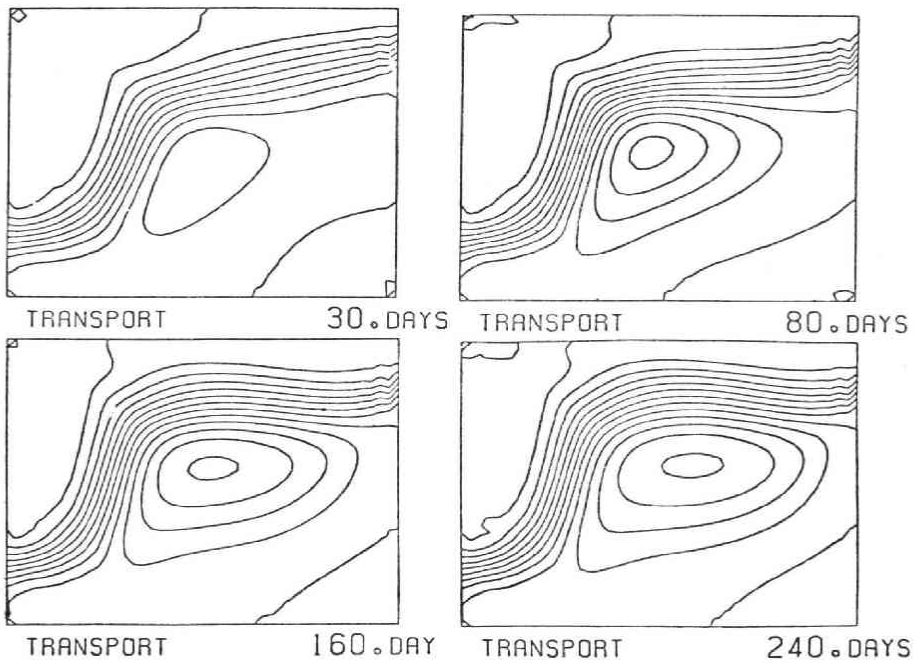

Fig. 5. Numerical evolutions of the transport function ϕ (Run 1). Contour interval is 2.5 Sv.

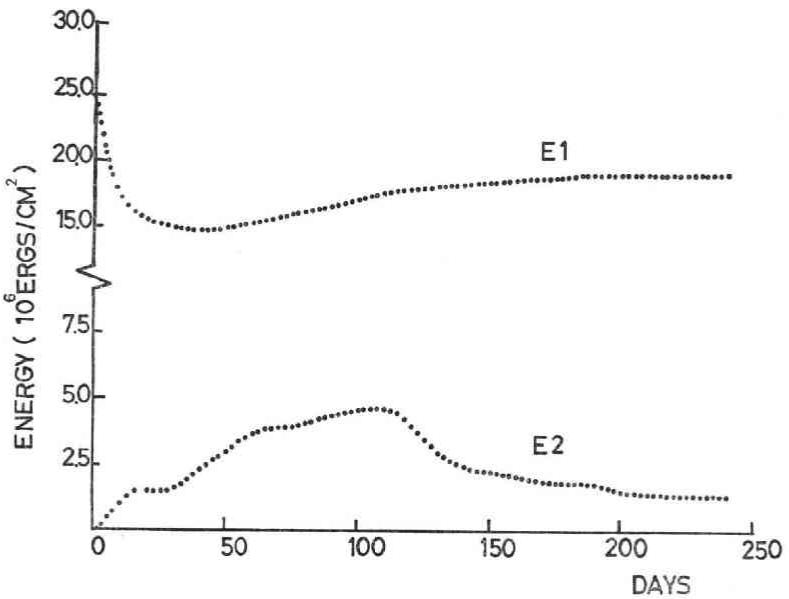

Fig. 6. Time change of the kinetic energy per unit area for the upper layer E1 and the lower layer E2.

initial flow path given by Fig. 4 moves westward to form a characteristic flow pattern in about 30 days, and the pattern shows little change after 80 days. The stability of the numerical solution has been examined by the temporal variation of the kinetic energy per unit area in the upper and the lower layers as E1 and E2, respectively (Fig. 6). The lower layer is at rest in the initial state, but a small movement is induced in it with the advance of time. The E2 attains to its maximum at about the 120th day, then diminishes monotonously to about 1/3 of the maximum value by the 240th day, while E1 approaches to its equilibrium value in about 180 days. It should be noticed

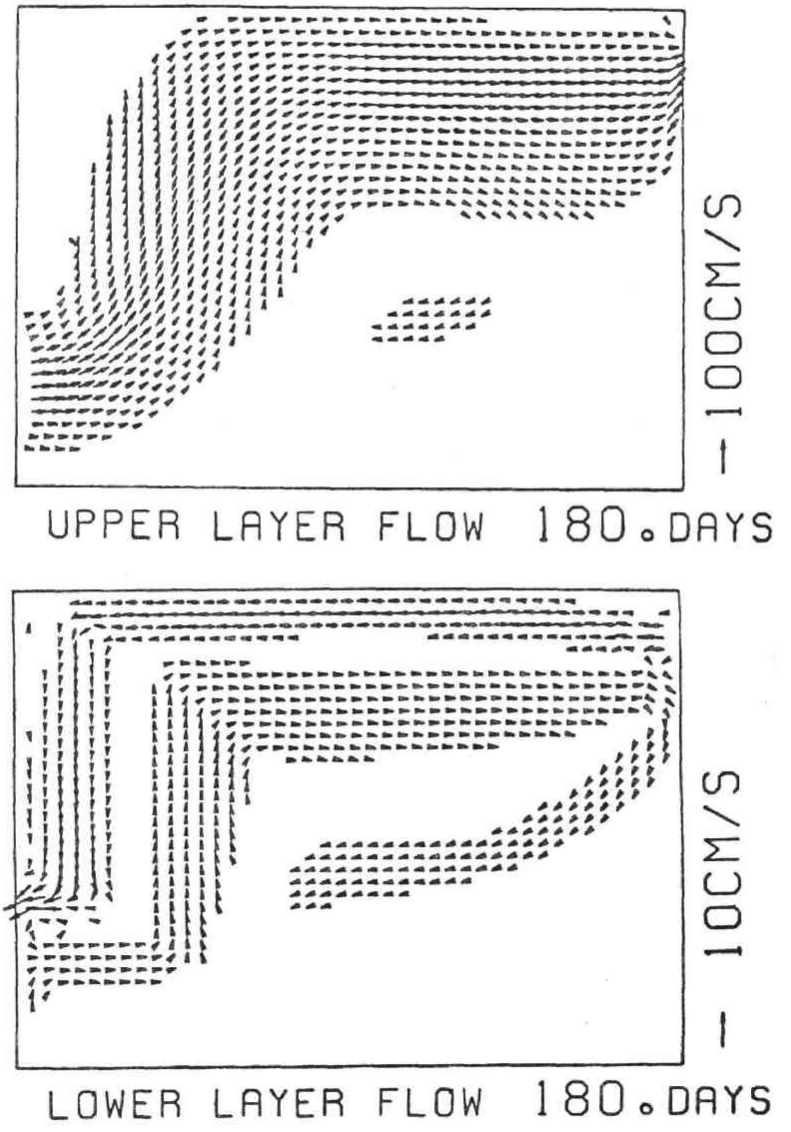

Fig. 7. Horizontal current velocity in upper and lower layers, indicated by velocity vectors. In these figures, only the dominant velocity vectors are drawn.

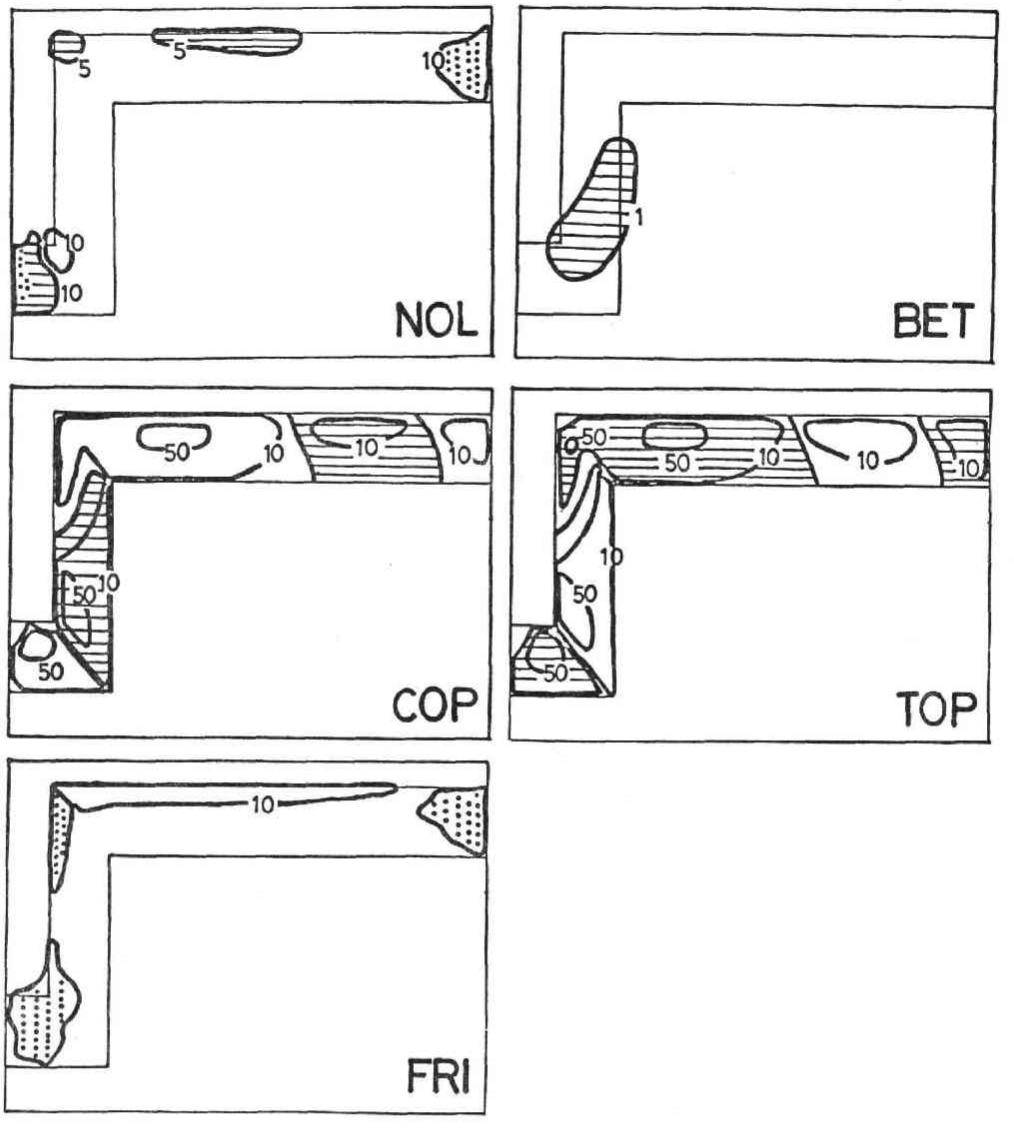

Fig. 8. (a)

that the flow pattern in Fig. 5 remains quasi-stationary while E2 experiences a large change between the 80th and 240th days. Also, the quasi-stationary flow path takes a somewhat aslant course, in contrast to the flow pattern of Fig. 9, which is the solution of Run 2 for no continental slope, and in which the flow path takes straight northward along the west coast.

The lower layer should achieve quiescence finally from the consideration of the conservation of potential vorticity (Rooth et al., 1978), since there is neither inflow and ouflow at the boundary in the lower layer, nor transfer of stress across the interface.

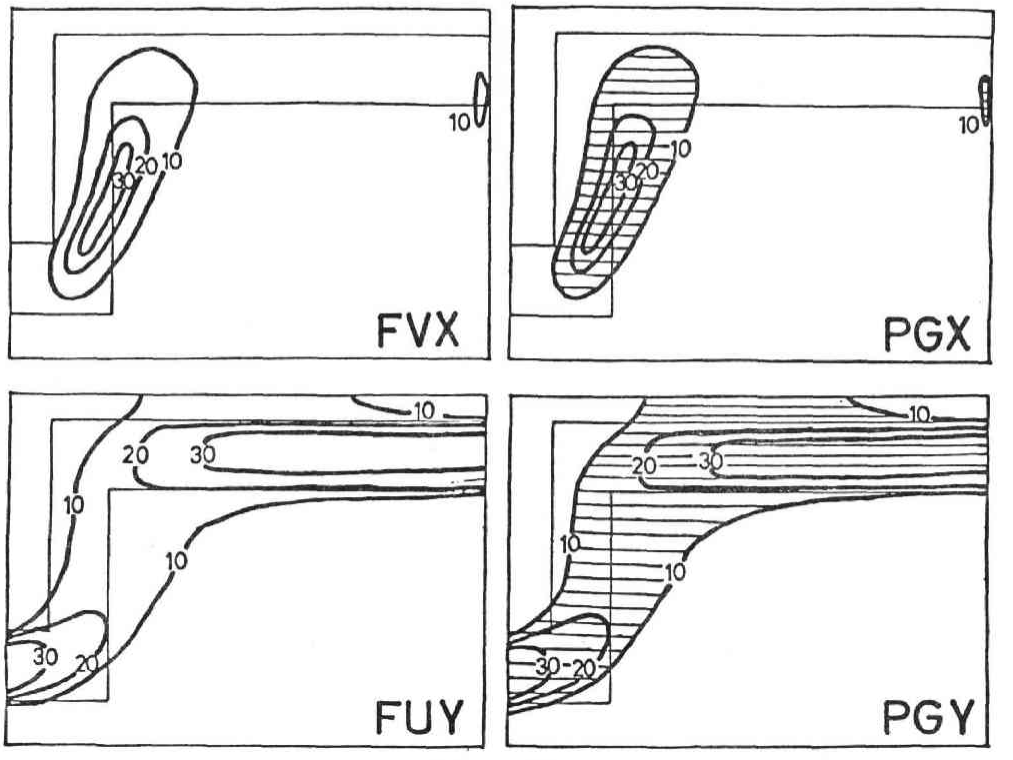

Fig. 8. (b)

Fig. 8. Regions of important contributions of each term to the total numerical solution. (a) Voriticity equation (9), (b) Shear equations (10) and (11). Symbols in the lower right part of each panel are same as in (9)–(11). Unit is 10^{-12} sec^{-2} in vorticity equation and 10^{-4} cm s^{-2} in shear equation. Shaded areas indicate negative contribution.

In this state, the geastrophic isostacy is attained, and the upper layer flow is unaffected by the topographic effect (Suginohara, 1980). The decrease of E2 in Fig. 6 seems to indicate the gradual approach to this state. However, the achievement of the geostrophic isostacy will need considerably large time.

The velocity fields of the upper and the lower layers at the 180th day are presented in Fig. 7. The scale of magnitude of the arrows for each layer is different, and only the dominant velocity vectors are drawn. The characteristic velocity along the upper layer flow is 70 cm s^{-1} whereas that of the lower layer is 3 cm s^{-1}. The main features of the upper layer are in close resemblance with those of the transport function. On the other hand, the lower layer currents, which are much weaker than those in the upper layer, approximately flow along the isopleth. More exactly, the lower layer flow pattern has a tendency to run along the contour line of f/h_2. This difference between the upper and the lower layer has also been shown in other two layer models including bottom topography (Miura and Suginohara 1980, Suginohara 1980), and these results may be regarded as the surface mode and the bottom mode proposed by Rhines (1970).

Now, the balance of the terms in the equations is examined. The spatial distributions of the balances among these terms at the 180th day are illustrated in Fig. 8 by use of the symbols indicated in (9), (10) and (11). In the vorticity equation for barotropic mode, the main balance exists between the topographic divergence term (TOP) and the topographic coupling term (COP). As to the terms in the shear equation, the geostrophic balance dominates, namely the pressure gradient term and the Coriolis term are well balanced as seen in Fig. 8 (b).

The topographic terms have 50 times larger magnitude than the planetary β term (BET), in spite of the fact that the characteristic velocity of the lower layer is only 5% of that of the upper layer. As already mentioned, the lower layer velocity should tend to zero eventually, and in this state, the topographic effect should vanish. As to the critical condition at which the topographic terms become smaller than the β term, an order estimation gives a velocity of the lower layer of 0.5% of that of the upper layer, or of the order of mm s^{-1}, as shown in the Appendix. It is expected that as long as the lower layer velocity has some value of the order of cm s^{-1}, the predominance of the main balance between the topographic terms lasts, and this state may correspond to the above mentioned quasi-stationary flow path. In the actual conditions of the Kuroshio, there are always some variations, and also the lower layer velocity of the order of cm s^{-1} (Worthington and Kawai 1972, Taft 1978). Consequently, it is expected that the predominance of the topographic terms also holds in the actual Kuroshio. In the case that the direction of the lower layer flow is opposite, the conclusion remains the same. From the above reasoning, we regard the numerical solution of from the 180th to the 240th day as the quasi-stationary flow path representative of the actual conditions of the Kuroshio.

The numerical solution obtained in this model is in a good resemblance to the observed current pattern of this region in spite of the poor approximation of coastal and bottom topographies. Especially, it is noticeable that the warm anticyclonic eddy in the offshores of Shikoku has been formed in this numerical model, corresponding to the observed features. Namely, Hasunuma and Yoshida (1978) proposed a long-term mean geopotential anomaly in the North Pacific Ocean as shown in their Fig. 1. They pointed out that this anticyclonic eddy in the offshores of Shikoku continued to exist stably with its center located about 34°N and 134°E. This eddy may be related to the anticyclonic eddy formed in the center part of this numerical model, and it may be associated with the anticyclonic circulation of the western boundary current generated by the coastal boundary and continental slope corresponding to this region.

Next, mention will be given as to the other additional runs for comparison with Run 1. The final result of the numerical solution of Run 2 in which the basin is flat is shown in Fig. 9 by the transport function. A strong northward current exists along the western boundary of the basin corresponding to the east coast of Kyushu. The principal dynamics of this narrow current is in the westward intensification. The vorticity balance in the final stage of this case is dominantly attained between the planetary β term (BET) and the frictional term (FRI) with the nonlinear term of supplementary

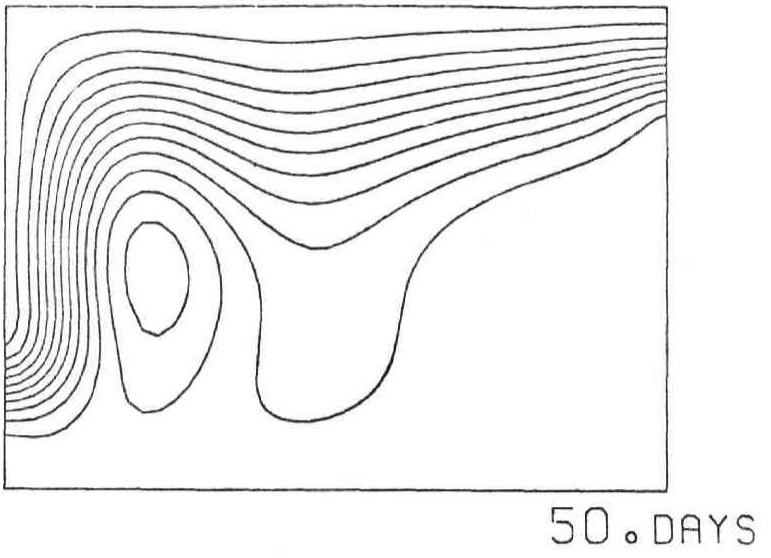

Fig. 9. Transport function ϕ for the case of Run 2. Contour interval is same as Fig. 5.

importance. The vorticity balance is similar to the case of Munk et al. (1950), which had a weak modification by the nonlinear term to the linear vorticity solution by Munk (1950). The influence arising from the exclusion of the continental slope is more prominent in the northern half domain. The width of the eastward current along the northern boundary is considerably wider than that of the basic model. The outflow boundary condition concentrates the interior wide current at the east end. While the northward strong current along the Kyushu in Run 2 is thus a consequence of the planetary β effect, it is inferred that the narrow current observed in the offshore of Shikoku in Run 1 may be due to the effect of bottom toporgaphy.

The volume transport function for Run 3 where the planetary β effect is lacking is shown in Fig. 10. In this case, the path along the continental slope is due to the topographic effect of the continental slope only. From the comparison of Figs. 9 and 10 also, our conclusion of the predominance of topographic terms in the quasi-stationary flow path in Run 1 is understandable.

The final case of Run 4 in which the density stratification is excluded (the barotropic model) is shown in Fig. 11. The flow is formed along the isopleths. The total flow pattern of this model has a close resemblance to that of the lower layer vleocity field of the basic model (see Fig. 7). The results may be explained by the conservation of the linearized potential vorticity f/D, which is due to the trapping of the kinetic energy along the slope by viscosity through continental shelf waves. The latitudinal change in f is not conspicuous: the current flows along the isopleths of the depth. This fact has already been revealed also in previous homogeneous models (Holland, 1967; Endoh, 1973; and Sekine, 1979). It should be noted here that the topographic effect is still influential as the bottom mode even in a two layer ocean, in their quasi-stationary flow as discussed in the basic model.

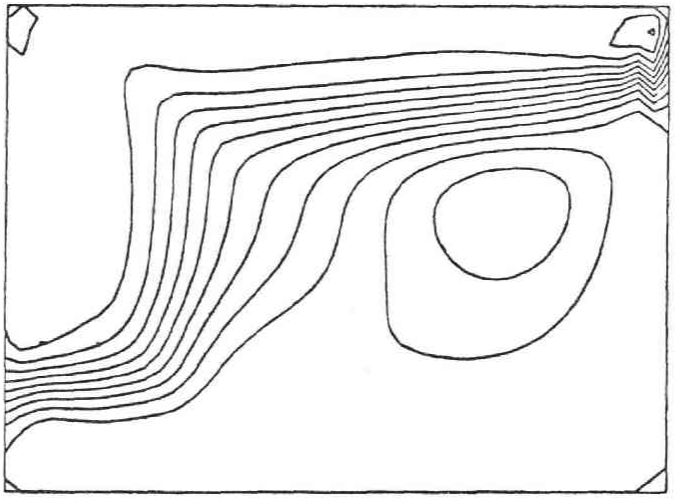

Fig. 10. Transport function ϕ for the case of Run 3. Contour interval is the same as in Fig. 5.

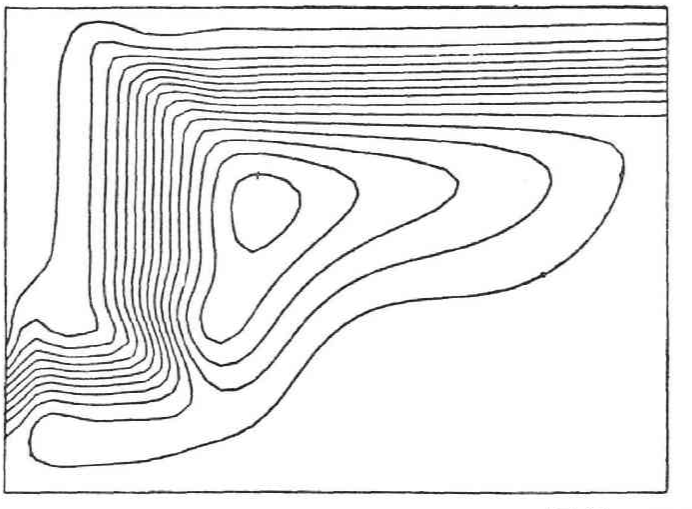

Fig. 11. Transport function ϕ for the case of Run 4. Contour interval is the same as in Fig. 5.

4. Discussion on the occurrence of the small meander

In this study, the path dynamics of the Kuroshio, between south of Kyushu and the offshores of Kii Channel, has been investigated numerically for the purpose of understanding the condition for the generation of the small meanders which are observed prior to the formation of a stationary large meander.

The main results of the last section are summarized as follows. The Kuroshio in the studied region has a stable path of flow along the continental margin in the

quasi-stationary state of no variation of the volume transport. The dynamical factors which force the Kuroshio path along the continental margin are the bottom effect of the continental slope and the planetary β effect. The contribution of the former on the path formation is more dominant than that of the latter, unless the velocity of the lower layer is much smaller than the order of 0.5% of the upper layer velocity. Since the path of flow is so stable under the balance of the topographic terms, the occurrence of small meanders as sometimes observed in the southeast of Kyushu seems to be very difficult, in the quasi-stationary state of the oceanic conditions.

From the above results, we should assume some causes for the occurrence of these small meanders. For the generation of them, it is necessary that the effects of the topography and the westward intensification are overcome. This may be expected in the excess of the inertia of the current due to the increase in the volume transport, especially, due to the increase in the upper layer velocity.

In fact, the order of magnitude of the accelerational terms can become comparable with that of the topographic terms, if a usually observed variations of the volume transport is introduced to the quasi-stationary state. Namely, if we assume that the relative vorticity z, 2×10^{-5} s^{-1} corresponding to the current with a maximum velocity of 100 cm s^{-1} and a half width of 5×10^{6} cm, and the current velocity increases by 50% in 10 days, the local change term $\partial z/\partial t$ becomes of the order of 10^{-11} s^{-1}. This is much larger than the magnitude of the planetary β term, and is comparable with that of the topographic effect terms estimated in Appendix.

Further studies from the side of the analysis of actual data, and also by numerical experiments including variation of the volume transport, will be reported elsewhere.

Acknowledgments: The authors would like to thank Dr. T. Sugimoto and other members of their Laboratory and Dr. N. Suginohara, University of Tokyo for their valuable discussions and comments. This study was performed as member of the Kuroshio Co-operative Research Group organized by Prof. T. Teramoto, University of Tokyo, and so partially supported by a Grant-in-Aid for Scientific Research by the Ministry of Education, Science and Culture, Project No. 234025. The numerical calculations were carried out on an ACOS-700 and ACOS-900 of the Computer Center of Tohoku University.

Appendix

A rough estimation for the critical condition at which the topographic effect becomes negligible in a two layer model is considered as follows.

The linearized vorticity equations for the upper layer and the lower layer can be written as

$$\frac{\partial z_1}{\partial t}+\beta v_1-\frac{f}{h_1}\frac{\partial}{\partial t}(\zeta+\eta)=A_h\nabla^2 z_1 \tag{A-1}$$

$$\frac{\partial z_2}{\partial t}+\beta v_2-\frac{f}{h_2}\left(\frac{\partial h_2}{\partial x}u_2+\frac{\partial h_2}{\partial y}v_2\right)+\frac{f}{h_2}\frac{\partial \eta}{\partial t}=A_h\nabla^2 z_2\,, \tag{A-2}$$

where

$$z_1 = \frac{\partial v_1}{\partial x} - \frac{\partial u_1}{\partial y}, \qquad z_2 = \frac{\partial v_2}{\partial x} - \frac{\partial u_2}{\partial y} \tag{A-3}$$

In the stationary state in which the lower layer has no motion. or the geostrophic isostacy, the main balance of the vorticity equation should be held between the planetary β effect (βv_1) and the viscous term ($A_h \nabla^2 z_1$) in the upper layer (A–1). In the transient state, the topographic effect is considered to be essential and its influence is represented by the third term of the left hand side of (A–2) and by the terms of the interface change including in (A–1) and (A–2). In our numerical model, the relative magnitude of the planetary β effect and the topographic β effect is compared as follows. From $|\beta| \simeq 2 \times 10^{-13}$ cm s^{-1} and $\left| \frac{f}{h_2} \nabla h \right| \equiv B_T \simeq 1 \times 10^{-11}$ cm s^{-1}, it is seen that the topographic effect is more dominant than the planetary β effect first in the lower layer motion. Then the topographic effect in the upper layer can be estimated by $\frac{f}{h_1} \frac{\partial \eta}{\partial t}$, and we may estimate this term by the assumption of the lower layer balance of

$$\frac{f}{h_2} \frac{\partial \eta}{\partial t} \simeq \frac{f}{h_2} \left(\frac{\partial h_2}{\partial x} u_2 + \frac{\partial h_2}{\partial y} v_2 \right) \tag{A-4}$$

and we get

$$\frac{f}{h_1} \frac{\partial \eta}{\partial t} = \frac{f}{h_1} \left(\frac{\partial h_2}{\partial x} u_2 + \frac{\partial h_2}{\partial y} v_2 \right) \tag{A-5}$$

The relative magnitude for the topographic effect and the planetary β effect can thus be compared from the upper layer equation (A–1) as

$$\beta v_1 \simeq 2 \times 10^{-13} v_1 \tag{A-6}$$

and

$$\frac{f}{h_1} \frac{\partial \eta}{\partial t} = \frac{h_2}{h_1} (B_T) v_2 \simeq 7 \times 10^{-11} v_2 \tag{A-7}$$

Accordingly, the topographic effect becomes negligible only when the lower layer velocity is much smaller than about 0.5% of the upper layer.

References

Bolin, B., 1950: On the influence of the earth's orography on the general character of the westerlies. *Tellus*, **2**, 184–195.

Endoh, M., 1973: Western boundary current crossing a ridge – barotropic and equivalent barotropic models – *J. Oceanogr. Soc. Japan*, **29**, 140–147.

Endoh, M., 1978: Effects of a marine ridge to western boundary current in a three-dimensional source-sink flow model. *J. Oceanogr. Soc. Japan*, **34**, 303–306.

Fukuoka, J., 1960: An analysis on the mechanism of the cold water mass appearance in the Enshu-nada. *The Oceanogr. Mag.*, **11**, 127–143.

Hasunuma, K. and K. Yoshida, 1978: Splitting of the subtropical gyre in the western north Pacific. *J. Oceanogr. Soc. Japan*, **34**, 160–171.

Holland, W.R., 1967: On the wind-driven circulation in an ocean with bottom topography. *Tellus*, **19**, 582–600.

Holland, W.R. and L.B. Linn, 1975: On the generation of mesoscale eddies and their contribution to the oceanic general circulation. I. A preliminary numerical experiment. *J. Phys. Oceanogr.*, **5**, 642–657.

Matsuno, T., 1966: Numerical integrations of the primitive equations by a simulated backward difference method. *J. Meteor. Soc. Japan*, **44**, 76–84.

Miura, H. and N. Suginohara, 1980: Effects of bottom topography and density stratification on the formation of western boundary currents Part I: Wind-driven general circulation model. *J. Oceanogr. Soc. Japan*, **35**, 215–223.

Moriyasu, S., 1961: On the influence of the monsoon on the oceanographic conditions. J. Oceanogr. Soc. Japan, **17**, 14–19.

Munk, W.H., 1950: On the wind-driven ocean circulation. *J. Meteorol.*, **7**. 79–93.

Munk, W.H., G.W. Groves and G.F. Carrier, 1950: Note on the dynamics of the Gulf Stream. *J. Mar. Res.*, **9**, 218–238.

Nitani, H., 1975: Variation of the Kuroshio south of Japan. *J. Oceanogr. Soc. Japan*, **31**, 154–173.

Rhines, P., 1970: Edge-, bottom-, and Rossby waves in a rotating stratified fluid. *Geophys. Fluid Dyn.*, **1**, 273–302.

Rooth, C., H. Stommel and G. Veronis, 1979: On motions in steady, layered, geostrophic models. *J. Oceangor. Soc. Japan*, **34**, 265–267.

Sekine, Y., 1979: A numerical experiment for bottom effect of the Izu ridge on Path of the Kuroshio I. Barotropic stationary model. *Sci. Rep. Tôhoku Univ.*, Ser. 5, Geophys., **26**, 67–80.

Shoji, D., 1972: Time variation of the Kuroshio south of Japan, in Kuroshio: Its physical aspects. edited by H. Stommel and K. Yoshida, Univ. Tokyo Press, pp. 217–234.

Solomon, H., 1978: Occurrence of small "Trigger" meanders in the Kuroshio off southern Kyushu. *J. Oceangor. Soc. Japan*, **34**, 81–84.

Stommel, H. and K. Yoshida, 1971: Some thoughts on the cold eddy south of Enshunada. *J. Oceanogr. Soc. Japan*, **27**, 213–217.

Suginohara, N., 1973: Response of a two-layer ocean to typhoon passage in the western boundary region. *J. Oceanogr. Soc. Japan*, **29**, 236–250.

Suginohara, N., 1980: Effects of bottom topography and density stratification on the formation of western boundary currents Part II: Inflow-outflow model. *J. Oceanogr. Soc. Japan*, **35**, 224–232.

Taft, B.A., 1978: Structure of Kuroshio south of Japan. *J. Mar. Res.*, **36**, 77–117.

White, W.B. and J.P. McCreary, 1976: On the formation of the Kuroshio meander and its relationship to the large-scale ocean circulation. *Deep-Sea Res.*, **23**, 33–47.

Worthington, L.V. and H. Kawai, 1972: Comparison between deep sections across the Kuroshio and the Florida Current and Gulf Stream, in Kuroshio: Its physical aspects. edited by Stommel, H. and K. Yoshida, Univ. Tokyo Press, pp. 371–385.